Conclusions

In this study it has been demonstrated that the AGA maneuver is dynamically unstable with respect to altitude errors. However, it has been shown that the instability may be controlled using feedback linearization. The existence of the instability further emphasizes the need for robust guidance during the atmospheric pass. Other related dynamical issues will be investigated in future studies.

References

[1]McRonald, A. D., and Randolph, J. E., "Hypersonic Maneuvring for Augmenting Planetary Gravity Assist," *Journal of Spacecraft and Rockets*, Vol. 29, No. 2, 1992, pp. 216–222.

[2]Randolph, J. E., and McRonald, A. D., "Solar System Fast Mission Trajectories Using Aerogravity Assist," *Journal of Spacecraft and Rockets*, Vol. 29, No. 2, 1992, pp. 223–232.

[3]Nonweiler, T. R. F., "Aerodynamic Problems of Space Vehicles," *Journal of the Royal Aeronautical Society*, Vol. 63, Sept. 1959, pp. 521–528.

[4]Van Buren, M. A., and Mease, K. D., "Aerospace Plane Guidance Using Time-Scale Decomposition and Feedback Linearization," *Journal of Guidance, Control, and Dynamics*, Vol. 2, No. 5, 1992, pp. 1829–1838.

Supersonic Axisymmetric Conical Flow Solutions for Different Ratios of Specific Heats

Bhavesh B. Patel,* B. K. Hodge,† and Keith Koenig‡
Mississippi State University,
Mississippi State, Mississippi 39762

Nomenclature

c_p = specific heat at constant pressure
c_v = specific heat at constant volume
h_o = stagnation enthalpy
M = Mach number
V_r' = dimensionless radial velocity, $V_r/V_{\max}$
V_θ' = dimensionless tangential velocity, $V_\theta/V_{\max}$
$V_{\max}$ = reference velocity, $\sqrt{2h_o}$
γ = ratio of specific heats, c_p/c_v
θ = polar coordinate in Eq. (1) or conical shock wave angle, deg
σ = cone semivertex angle, deg

Introduction

A NUMBER of sources[1,2] contain tabulations and charts for many useful compressible flow situations. For example, Refs. 1 and 2 both provide charts for conical supersonic flow of a calorically perfect gas over axisymmetric sharp cones with attached conical shock waves for a single ratio of specific heats, $\gamma = c_p/c_v = 1.405$ for Ref. 1 and $\gamma = 1.4$ for Ref. 2. Each contains sequences of charts with shock-wave angle, cone surface pressure coefficient, and cone surface Mach number vs cone semivertex angle, parameterized with freestream Mach number. No complementary study of conical flow has been reported for a variety of values of the ratio of specific heats.

Conical flows with different values of the ratio of specific heats are of interest because different gases have different specific heats ratios. Monatomic gases, such as helium, possess the largest value of γ, 1.67; diatomic gases, such as nitrogen and oxygen, and mixtures of diatomic gases, such as air, possess a ratio of specific heats of 1.4. The smallest value of γ is near unity for gases composed of very complex molecules. The value of $\gamma = 1.000001$ (hereinafter written as 1.0^+) represents the lower limiting case considered in this Note and is presented for completeness and as a demonstration of the robustness of the numerical technique.

The purpose of this Note is to summarize salient behavioral characteristics of calorically perfect conical supersonic flows for different values of the ratio of specific heats. A complete set of charts following the format of Ref. 1 is available in Patel et al.[3] Although the computation of such conical flows is relatively straightforward, some effort is required to assemble a useful set of information for a variety of values of γ. Over the possible range of the ratio of specific heats, $1.0^+ < \gamma < 1.67$, the characteristics show considerable variations.

Conical Supersonic Flow

A schematic of conical supersonic flow is presented in Fig. 1. A supersonic conical flowfield is defined by the following: 1) the shock wave is attached to the vertex of the cone, 2) the shock wave is conical in shape, 3) all flow properties are constant along radial lines, and 4) the flow between the shock wave and the cone surface is isentropic. The oblique shock relations hold across the conical shock wave. Conical supersonic flows were first solved graphically by Busemann[4] in 1929. In 1933, Taylor and Maccoll[5] derived the usually accepted conical flow equation,

$$\frac{\gamma-1}{2}\left[1-V_r'^2-\left(\frac{dV_r'}{d\theta}\right)^2\right]\left[2V_r'+\frac{dV_r'}{d\theta}\cot\theta+\frac{d^2V_r'}{d\theta^2}\right]-\frac{dV_r'}{d\theta}\left[V_r'\frac{dV_r'}{d\theta}+\frac{dV_r'}{d\theta}\frac{d^2V_r'}{d\theta^2}\right]=0 \quad (1)$$

and solved it numerically. Indeed, Anderson[6] views their paper and their numerical solution of Eq. (1), the Taylor-Maccoll equation, as a seminal point in the history of compressible flow. One of the first reported uses of digital computers in aerodynamics was the conical supersonic solutions of Kopal[7] that formed the basis of the charts in Ref. 1. Even after Kopal's report and the charts in Ref. 1, interest continued in such flows, and details of the flowfield about cones in supersonic flow were later tabulated by Sims.[8] Brower[2] provides additional historical details of the genesis of supersonic conical flow solutions.

The Taylor-Maccoll equation is an ordinary, nonlinear, second-order differential equation. The complexity of the differential equation precludes a closed-form solution. The results in this Note were

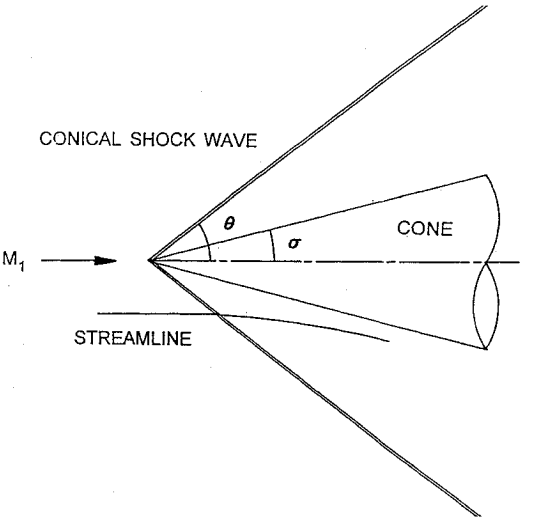

Fig. 1 Supersonic conical flow schematic.

Received June 18, 1993; revision received Sept. 7, 1993; accepted for publication Sept. 7, 1993.

*Undergraduate, Department of Aerospace Engineering; currently Graduate Research Assistant. Student Member AIAA.

†Professor, Department of Mechanical Engineering. Associate Fellow AIAA.

‡Professor, Department of Aerospace Engineering. Member AIAA.

generated using a fourth-order Runge-Kutta method to solve the differential equation.

Most numerical techniques used to solve the Taylor-Maccoll equation integrate from the cone surface to the shock wave or from the shock wave to the cone surface. The conical flow characteristics presented herein were obtained by integrating from the shock wave to the cone surface. For a given conical shock-wave angle, the conditions across the shock wave were determined using the oblique shock relations, and the integration process started downstream of the conical shock wave. Small integration step sizes, $\Delta\theta = 0.01$ deg, and double precision arithmetic (when using a 32-bit machine) were required, especially for low Mach numbers and small cone angles. At every integration step, the value of the dimensionless tangential velocity V'_θ was determined. The vanishing of V'_θ indicated that the cone surface had been reached, which thus defined the cone semivertex angle, and the integration process was terminated. The program was validated by replicating the conical supersonic flow charts of Ref. 1.

Results

Conical supersonic solutions (weak shock only) were obtained for ratios of specific heats of 1.0^+, 1.1, 1.2, 1.3, 1.4, 1.5, 1.6, and 1.67. The 48 full-page figures required to provide charts with sufficient clarity for practical use for the eight different ratios of specific heats considered are given in Ref. 3.

The real question, of course, is whether the specific heats ratio has important effects on the characteristics of conical supersonic flows. Angles larger than the maximum cone semivertex angle for an attached conical shock wave are associated with detached shock wave structures that are not conical. The maximum cone semivertex angle for an attached conical shock wave is often called the conical shock detachment angle. Similarly, the maximum wedge angle for an attached, planar oblique shock is called the wedge shock detachment angle. Because of the three-dimensional relieving effect associated with an axisymmetric flow vs a planar flow, the conical detachment angle is larger than the wedge detachment angle at a given upstream Mach number. Some compressible flow textbooks, Anderson,[6] for example, contain graphic representations of the maximum cone semivertex angle and the maximum wedge angle for attached shock waves for $\gamma = 1.4$ as a function of upstream Mach number. The analogous presentations for ratios of specific heats of 1.0^+, 1.2, and 1.67 are given in Fig. 2. This figure immediately answers the question of the significance of the ratio of specific heats on supersonic conical flowfields. Although the same trends are evident with upstream Mach number, the smaller the value of the ratio of specific heats the larger the shock detachment angle for a given upstream Mach number. Moreover, the smaller the value of the specific heats ratio, the smaller the difference between the cone and wedge shock detachment angles for a given upstream Mach number. The asymptotic behavior of shock detachment angles for the cone and wedge is also dependent on the ratio of specific heats. For example, the asymptotic nature of the $\gamma = 1.67$ behavior is evident at a much smaller upstream Mach number than is the asymptotic behavior for $\gamma = 1.0^+$.

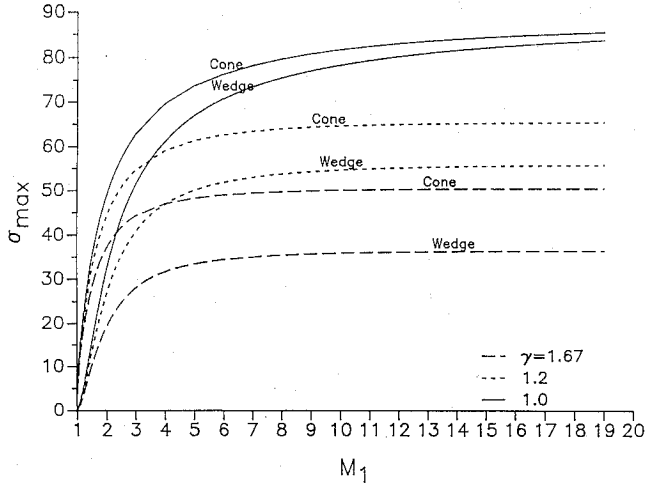

Fig. 2 Comparison of the conical and wedge shock detachment angles for $\gamma = 1.67$, 1.2, and 1.0^+.

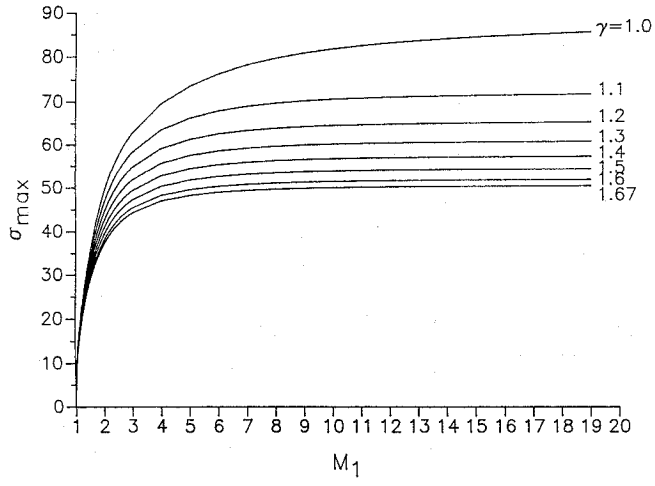

Fig. 3 Conical detachment angles for the ratios of specific heats investigated.

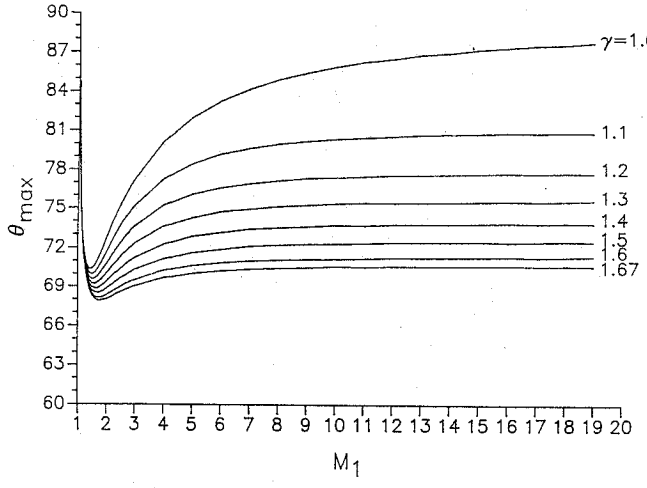

Fig. 4 Shock-wave angles for the conical detachment angles of Fig. 3.

If the conical shock detachment angle is plotted as a function of upstream Mach number for each of the ratios of specific heats, then Fig. 3 results. As the ratio of specific heats is increased from 1.0^+ to the limiting value of 1.67, the distinctions between the behavior in increments of ratio of specific heats of 0.1 diminish.

The conical shock-wave angles that correspond to the conical shock-wave detachment angles of Fig. 3 are also of interest. These shock-wave angles are identified as θ_{max} and are plotted in Fig. 4 as a function of upstream Mach number with the ratio of specific heats as a parameter. As in the previous figures, the ratio of specific heats is observed to exhibit an important effect on the behavior of the conical flowfield. For upstream Mach numbers close to one, the conical shock wave is nearly a normal shock wave, regardless of the ratio of specific heats. As the upstream Mach number is increased from near unity, the conical shock-wave angle associated with the conical shock-wave detachment angle reaches a minimum, and then increases monotonically as Mach number increases. The effect of the specific heats ratio on the shock-wave angle corresponding to the conical shock-wave detachment angle is especially significant for the lower values of the ratio.

Conclusions

As Figs. 2–4 demonstrate, the specific heats ratio has significant effects on the behavior of conical supersonic flowfields. The differ-

ences between the planar and conical shock-wave detachment angles and behavior become greater as the ratio of specific heats decreases from 1.67 to 1.0^+. The usually available results for $\gamma = 1.4$ are not good approximations over the possible range of ratio of specific heats. A complete set of charts, in the format of Ref. 1, is available in Patel et al.[3] for $\gamma = 1.0^+$, 1.1, 1.2, 1.3, 1.4, 1.5, 1.6, and 1.67.

References

[1]Anon., "Equations, Tables, and Charts for Compressible Flow," NACA TR-1135, 1953.

[2]Brower, W. B., *Theory, Tables, and Data for Compressible Flow*, Hemisphere, New York, 1990.

[3]Patel, B. B., Hodge, B. K., and Koenig, K., "Addendum to AIAA Paper 93-0970 Supersonic Axisymmetric Conical Flow Charts for Different Ratios of Specific Heats," Rep. TFD-93-1, Mechanical Engineering Dept., Mississippi State Univ., MS, Jan. 1993.

[4]Busemann, A., "Drucke auf Kegelformige Spitzen bei Bewegung mit Uberschallgeschwindigkeit," *Zeitschrift für Angewandte Mathematik und Mechanik*, Vol. 9, 1929, p. 496.

[5]Taylor, G. I., and Maccoll, J. W., "The Air Pressure on a Cone Moving at High Speed," *Proceedings of the Royal Society of London, Series A: Mathematical and Physical Sciences*, Vol. 139, 1933, pp. 278–311.

[6]Anderson, J. D., *Modern Compressible Flow with Historical Perspective*, 2nd ed., McGraw-Hill, New York, 1990.

[7]Kopal, Z., "Tables of Supersonic Flow Around Cones," Massashusetts Inst. of Technology, Boston, MA, MIT Center of Analysis Rep. TR-1, 1947.

[8]Sims, J. L., "Tables of Supersonic Flow Around Right Circular Cones at Zero Angle of Attack," NASA SP-3004, 1964.

Removal of Orbital Debris from Low Earth Orbit by Laser-Generated Drag

Mengu Cho*
Kobe University, Kobe 657, Japan

I. Introduction

In the near future, human space activities will result in significant increases in spacecraft size and the operational time in the orbit. One important issue to be resolved before this new era of the space development is the collision between spacecraft and orbital debris. In low Earth orbit the quantity of man-made orbital debris exceeds the number of natural meteoroids.[1] The pieces of debris that range from 1 to 10 cm are the most threatening because although they are too small to detect from the ground they are too large to shield. In this paper, we propose a method to remove the orbital debris of $1 \sim 10$ cm from low Earth orbit. We propose the use of laser pulses to generate drag to the debris; the orbital altitude will be lowered until the debris enters Earth's atmosphere and is burned up because of atmospheric heating.

It has long been known that a giant laser pulse irradiated to solid surface can produce thrust. The concept of using such a thrust for rocket propulsion is not new. Kantrovitz proposed the use of a laser beam to launch a rocket from the ground.[2] The principle of the debris deceleration is the same as the laser rocket propulsion. The pulse of a laser is radiated from a laser satellite to a solid target. Then the target surface is heated by the laser beam, the surface material vaporizes, and plasma is ignited in the vapor that absorbs the laser energy further. The high-temperature gas expands into a vacuum, converting the thermal energy into kinetic energy. The momentum of the hot gas is given to the remaining mass of the debris, just as in usual rocket propulsion.

In the present Note, we first describe the basic specifications of the laser satellite system. Second, we do numerical simulations of the debris removal to calculate how much laser energy is needed to remove the debris. Third, we discuss our findings.

Received Jan. 15, 1993; revision received May 14, 1993; accepted for publication July 12, 1993.

*Research Associate, Graduate School of Science and Technology. Member AIAA.

II. System Specification

A schematic picture of the laser satellite system is shown in Fig. 1. We propose to put a laser satellite into the Earth-circulating orbit at 700-km altitude. This altitude is chosen because the debris mainly is distributed within a 300–1100 km altitude.[1] The range of a laser beam is assumed to be 500 km, so one satellite can cover the entire area. The satellite power is provided by 25 kW solar arrays. We distribute 20 kW to the laser power supply and 5 kW to other, housekeeping uses, including the telescope operation. Because the satellite cannot always find debris, a battery is used to store the electricity while the laser is not operating. Assuming that the maximum operational rate of the laser is 10%, the laser can use 200 kW on average. For a laser efficiency of 5%, the laser average output is 10 kW.

As the laser source, we choose a 0.25 μm KrF excimer laser, because of its high power output and short wavelength. The laser beam is pointed by a gimbaled telescope. The laser pointing accuracy of 0.1 μrad is assumed, which is technically challenging but not impossible, judging from the state of art of the laser intersatellite communication.[3] As the spot diameter, weassume 0.1 m at 500 km distance. This spot can be made by a mirror of 1.6-m diam at the satellite. The spot diameter at the target is adjusted so that

$$d_{\text{spot}} = 1.27(\lambda R / D_{\text{mirror}}) \tag{1}$$

where $\lambda = 0.25$ μm, $D_{\text{mirror}} = 1.6$ m, and R is the distance to the debris. The minimum spot diameter is set at 1 cm because if we focus the laser beam too much, the resulting vapor pressure might exceed the material strength of the target material, thus producing more debris.

To deliver the appropriate momentum to the target, the target surface must be vaporized and plasma must be ignited. Reference (4) shows the momentum change of several materials induced by KrF laser irradiation. The momentum change becomes significant for a laser fluence higher than 3×10^4 (J/m^2). Below this fluence, the laser intensity is not strong enough to cause the vapor breakdown. Because the spot diameter at 500 km is 0.1 m, we assume 500 J as the laser energy per pulse and 50 ns as the pulse time. Then the laser intensity at the target is $I_L = 10^{12}$ (W/m^2). Because the laser can use 200 kW in the operation, the repetition frequency is 20 pps.

We now discuss the pointing and tracking scheme. The debris is first detected by the onboard telescope. The telescope, with 1.6 m aperture diameter can detect debris as small as 1 cm from a 500-km distance by detecting the visible solar reflection with a charge coupled device (CCD) sensor. The field of view of one CCD pixel must be large enough to keep the object within view while it accumulates the electric charges. Therefore, the debris orbit still has a large uncertainty of 10–100 μrad, depending on the field of view of one CCD pixel. Once the debris is detected, the fine pointing is made by laser radar using the KrF laser A in Fig. 1. The probable positions of the debris masses are scanned by the laser pulses, and the light reflection is measured by the UV detector. After the debris orbits are determined within the accuracy of 0.2 μrad, a giant laser pulse is shot from the KrF laser B to generate drag. Once drag is given to

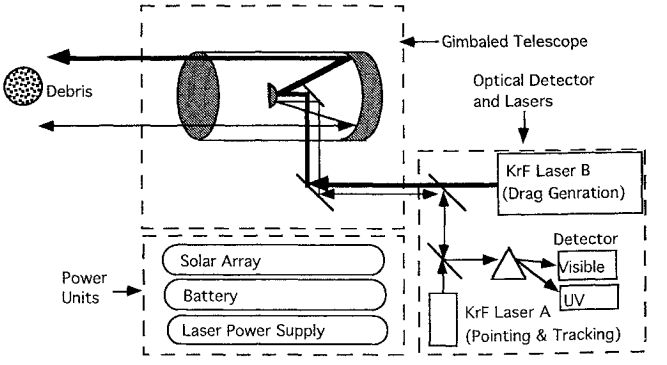

Fig. 1 Schematic picture of debris-removal laser satellite.